



ME6108 Project Final Report

Students

JIANG ZONGHENG A0191684U
ZHANG WANG A0284866
SHEN YIXIU A0263954U
WEI HUANXIA A0285164Y

Supervisors

Prof Lee Heow Pueh
Prof Lim Kian Meng

10 Nov 2023

Department of
Mechanical Engineering
National University of Singapore

Abstract

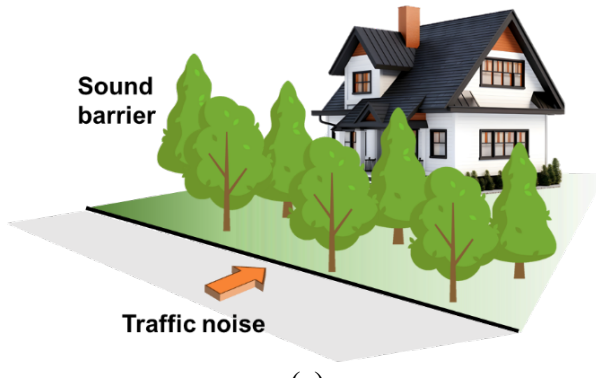
This study explores the design, simulation, fabrication, and application of sonic crystals for acoustic shielding. Utilizing the linearized wave equation as the key governing equation for acoustic simulations, the research evaluates the role of specific structures, such as fractal patterns, fluidic attributes, and square C interleave shapes, when integrated with sonic crystals. Preliminary results demonstrate that these structures, combined with sonic crystals, show significant sound shielding properties at selected frequencies. Moreover, gaps within these structures significantly influence sound pressure dynamics due to interactions between incident and reflected sound waves. Furthermore, the study delves into the unidirectional acoustic characteristics of sonic crystals, revealing similar insertion losses in both directions at specific frequencies. Based on simulation outcomes, high-performing sonic crystals are selected for 3D printing and tested in the Acoustic Lab. Comparisons between experimental and simulation results are done and analyzed.

1 Introduction

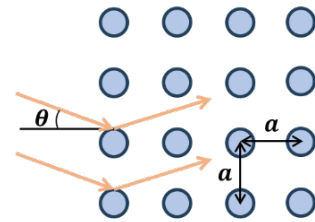
With the advancements in acoustical science, our understanding has transcended beyond the basic principles of sound propagation, delving into the intricate manipulation of acoustic waves through tailored materials and topological structures. This manipulation encompasses a wide spectrum of acoustic phenomena including absorption, filtration, modulation, diffraction, and propagation of sound waves [1-3]. Through specific material and structural choices, intentional interference with the behavior of sound waves has been made possible, paving the way for a myriad of practical applications. For instance, engineered acoustic barriers can be devised to efficiently attenuate or isolate noise within particular frequency ranges [4-6]. In the realm of sensor technology, the modulation of acoustic waves enables precise detection of various physical parameters [7, 8]. Additionally, research

into sonic architectural structures offers opportunities for optimized acoustic performance in reverberation building design [9], catering to both improved musical venues and heightened comfort in expected required spaces [10]. Furthermore, emerging interdisciplinary fields, such as acoustic metamaterials [2, 11] and sonic crystals [12-14], have expanded the horizon of possibilities, allowing for sound manipulation in ways previously deemed unattainable.

Sonic Crystals, comparable to photonic crystals in the field of optics, are specialized mediums composed of periodically distributed scatterers [15]. Their unique propagation qualities for acoustic waves have opened an abundance of utilizes in acoustics, electronics, and other associated domains. Notably, its employment in sound isolation [13], acoustic lenses [16], and waveguides [17] has been widespread. A defining aspect of sonic crystals is their capacity to manifest an acoustic band gap,



(a)



(b)

Fig 1. (a) Tree sound barriers, and (b) schematic of sonic crystal alignment.

a precise frequency range where sound waves cannot propagate effectively within the crystal. The formation of this band gap is attributed to the interference and scattering of sound waves by the scatterers within the crystal. For sonic crystals with a regular and periodic arrangement, especially in sound barriers intentionally arranged with trees or cylindrical sculptures [18, 19] as shown in **Fig 1(a)**, Bragg's law can serve as a preliminary tool to predict the approximated occurrence of acoustic band gaps, shown as **Eq 1**.

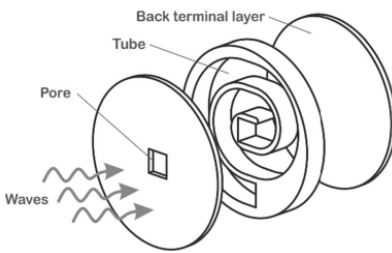
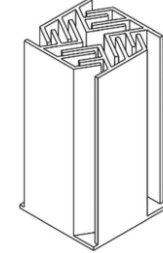
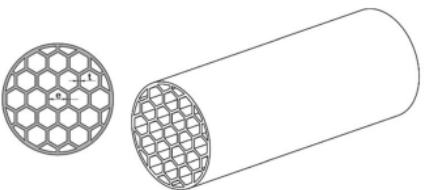
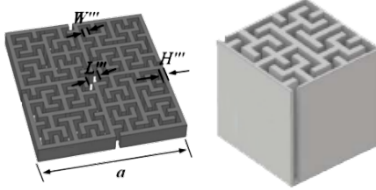
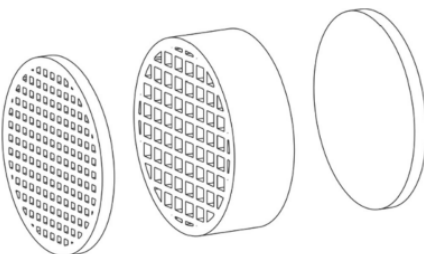
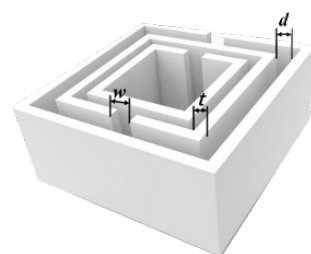
$$m\lambda_s = 2a \sin(\theta) \quad (1)$$

Where λ_s is the wavelength of sound gap, can be converted into frequency with local sound speed. m is scattering order. a is the lattice constant defined as the distance between adjacent scatters shown as **Fig 1(b)**. θ is sound incident angle. Benefiting from the evolution of material science and the emergence of additive manufacturing techniques [1], the study of sonic crystals has transcended basic arrangements and filling fraction

methodologies. By assimilating sophisticated spatial geometries, topological patterns, and porous designs, there has been a successful fusion of inventive components like Helmholtz resonators [20], micro-perforations [21], and damping layers [22]. Consequently, this has culminated in the rapid development as researchers incorporate more features into sonic crystals that demonstrate superior and more tunable frequency band gaps

As researchers incorporate more features into scattering entities, two primary orientations emerge: radial and axial. In axial studies, a coplanar spiral structure embedded within a tube, paired with a Helmholtz resonator, showcased enhanced absorption rates near 250Hz [23]. Studies on periodic structures reveal that while shape exerts minimal influence on absorption coefficients, the impact of unit configuration and filling intricacy is pronounced [25]. Additionally, multilayer arrangements realized through 3D printing, offer compact and efficient acoustic metamaterial elements with high absorption coefficients [28]. Compared to

Tab 1. Specific sonic crystal shape in previous research.

Axially	Radially
<p>Coplanar spiral tube [23]</p> 	<p>Labyrinthine metamaterials [24]</p> 
<p>Periodic structures [25]</p> 	<p>Hilbert fractal [26, 27]</p> 
<p>Multilayer arrangement [28]</p> 	<p>Split tubes [29]</p> 

previous labyrinthine structures, tapered or spiral channels have significantly improved impedance matching [24]. Owing to the Hilbert curve's efficient spatial-filling properties and intricacy within fractal domains, it has garnered attention in thin-walled sonic crystals. Furthermore, it can induce multiple peaks of acoustic pressure loss, leading to multi-band gaps [26, 27]. Lastly, the split tube, as a tunable acoustic metamaterial, offers a novel approach by flexibly and selectively adjusting noise reduction frequencies [29].

Inspired by these foundational studies, we intend to explore and compare four intriguing models through both simulation and experimental approaches. We'll investigate one-dimensional filling curves based on fractal space mathematical models, specifically the Hilbert curve and Gosper curve, which offer controllable spatial complexities. We will also delve into the Tesla valve structure barrier, inspired by unidirectional fluid flow, and study the square C-type split interleave structure under varying characteristic attributes.

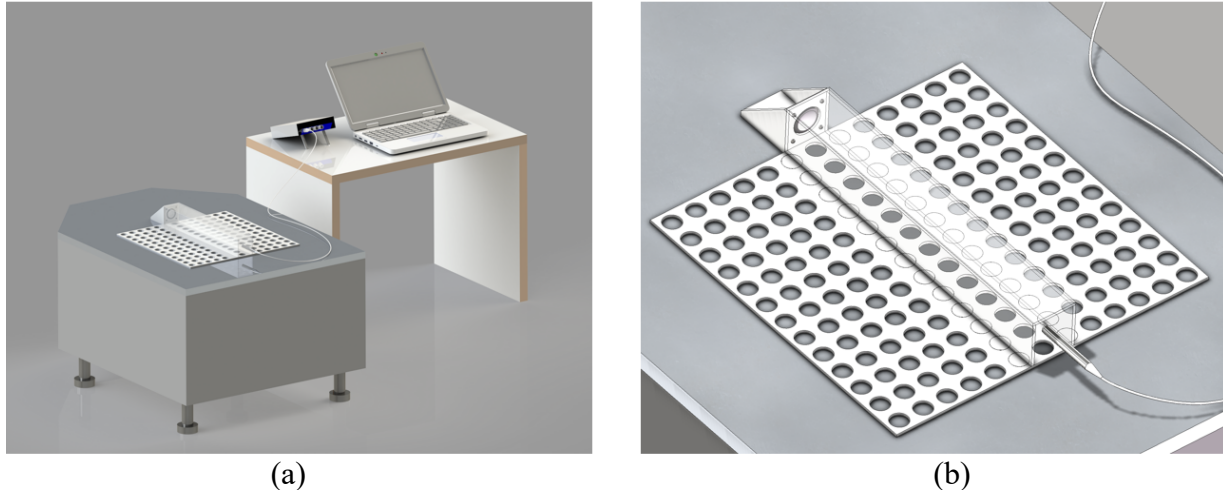


Fig 2. (a) Experiment setup schematics, (b) zoom-in picture of acoustic testing section.

2 Methodology

2.1 Design

The above-mentioned 4 different sonic crystals will be designed, simulated, and manufactured for experiment verification. To confirm the overall size of the sonic crystals to be designed, the real experiment setup is measured and modeled.

The experiment setup consists of a test bench and a data recording device connected to a laptop. Sonic crystals can be installed in different layouts on the acrylic plate with periodic holes, as shown in Fig 2. Acoustic waves of different frequencies coming from the speaker on the left top of **Fig 2(b)** will be collected by a microphone on the right bottom of **Fig 2 (b)**.

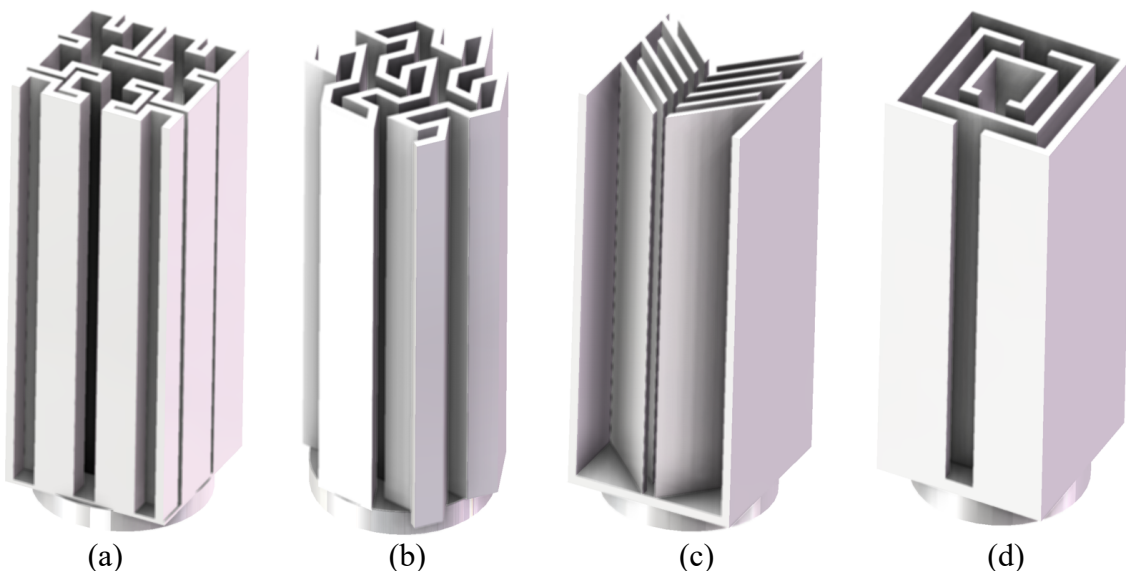
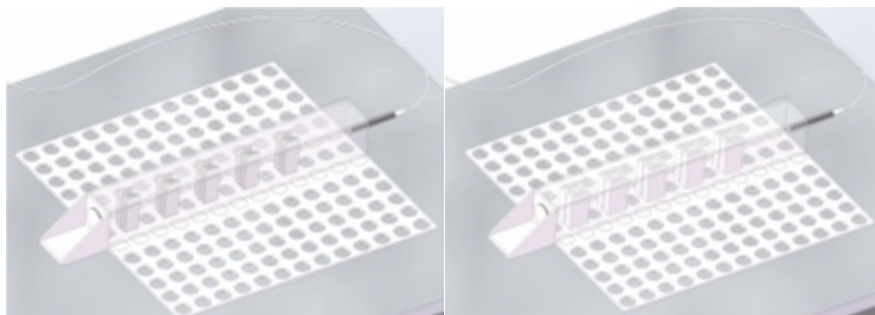


Fig 3. The models of used structures. (a) Hilbert curve structure. (b) Gosper curve structure. (c) Tesla valve structure. (d) C-type square split interleave structure.



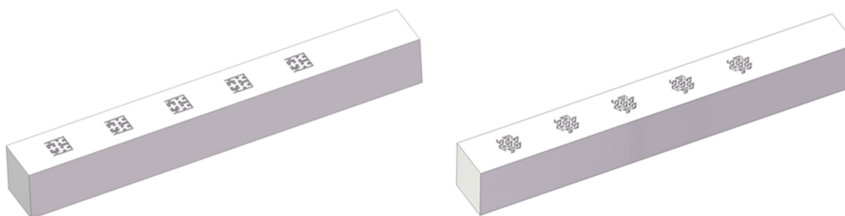
(a)

(b)



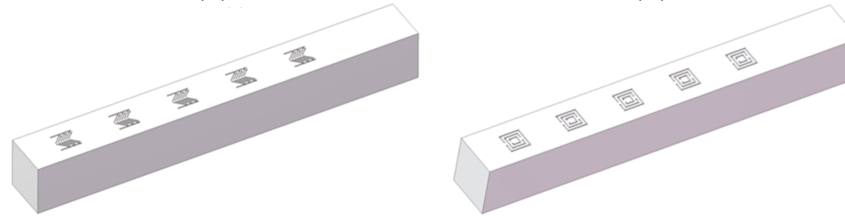
(c)

(d)



(a)

(b)



(c)

(d)

Fig 4. Test layout of **(a)** Hilbert curve structure, **(b)** Gosper curve structure, **(c)** Tesla valve structure, and **(d)** C-type square split interleave structure.

Fig 5. 3D design for simulation of **(a)** Hilbert curve structure, **(b)** Gosper curve structure, **(c)** Tesla valve structure, and **(d)** C-type square split interleave structure.

According to the measurements, the acrylic cuboid testing section in **Fig 2 (b)** is 560 mm × 67 mm × 77 mm (L × W × H). The bottom square acrylic plate has periodic holes of 30 mm with a depth of 5mm. The distance between two neighboring holes is around 86 mm. The 4 types of sonic crystals are designed to have an effective height of 75 mm with

another 4.5 mm cylindrical base for easier mounting, and the width is around 30mm. Each of the 4 types of sonic crystals will be put into the experiment setup periodically for testing in comparison with the simulation results, shown in **Fig 4**. This experimental design allows us to exclude most of the designs and parameters that perform unsatisfactorily

in the simulation session, and to test and delve into other better designs in the experiment.

The simplified 3D designs for each type of sonic crystals presented in the cuboid testing section have been crafted to facilitate more straightforward simulation processes. These designs retain the essential characteristics and functionalities of the original sonic crystals, while being modified for ease of simulation in a 3D environment. The focus in creating these designs has been on maintaining the accuracy of the sonic properties and interactions within the cuboid testing framework, ensuring that the simulations provide reliable data for further analysis (**Fig 5**).

Hilbert curves are fractal patterns that offer a unique and controllable means of influencing the behavior of sound waves, encompassing their transmission, reflection, and absorption characteristics. As per the findings in current research, Hilbert curves possess distinctive attributes such as multi-band sound blocking capabilities, the potential for achieving negative mass density and bulk modulus when applied in acoustic contexts [28]. These attributes open up avenues for the realization of a range of unconventional acoustic phenomena.

The article [28] also includes calculations that underscore the minimal impact of principles like Helmholtz resonance on fractal patterns such as Hilbert curves.

The Gosper curve, recognized as the ‘flowsnake’ or ‘Peano-Gosper’ curve, is a space-filling fractal that exhibits unique geometric properties.[30] In our sonic

crystal research, the fractal attributes of the Gosper curve introduce intriguing possibilities for acoustic manipulation.

A Tesla valve is a specialized valve design typically composed of a series of circular or spiral baffles. These baffles are precisely engineered with specific geometric configurations to control the flow of fluid in a highly orchestrated manner as it passes through the valve.

The manipulation of fluid velocity through these tailored structural features holds significant utility in various applications, including pressure reduction systems, flow control, and the controlled modulation of heat transfer by adjusting fluid flow. It is conjectured that fluidic structures such as Tesla valves could be leveraged in the design of acoustic structures to optimize the transmission and propagation of sound waves. Notably, symmetric Tesla valve structures have demonstrated superior unidirectional flow characteristics in prior research, thereby encouraging the incorporation of symmetrical Tesla valve units to enhance acoustic performance.

The square split tubes exhibit distinctive resonant properties, making them particularly suitable for manipulating and attenuating acoustic waves [29]. There are three main parameters in the adopted design, which are slot width, wall thickness, and gap distance between walls. We speculate that changes in these three parameters may have a large impact on their acoustic properties. Therefore, parameters are changed and compared in the following simulations.

2.2 Simulation

The computational acoustic simulation is a powerful tool based on computer-aided engineering (CAE) and numerical calculations. It translates engineering problems into calculations through a series of mathematical models and control equations, providing researchers with relatively accurate results.

The computational acoustic simulations were conducted with the help of COMSOL, a multi-physics simulation platform. The solving process is under the description of a series of governing equations. The key governing equation of acoustic simulation is the linearized wave equation. In a homogenous, isotropic medium, given by Eq 2.

$$\nabla \cdot \left(-\frac{1}{\rho_c} (\nabla p_t - q_d) \right) - \frac{k_{eq}^2 p_t}{\rho_c} \quad (2)$$

Where p_t is the acoustic pressure variation at current solution time, given by **Eq 3**, and c is the speed of sound in the medium (hereby it presents the speed of sound in the air, namely around 343 m/s), ρ_c is dielectric characteristic impedance, k_{eq} is the wavenumber, given by **Eq 4**.

$$p_t = p + p_b \quad (3)$$

$$k_{eq}^2 = \left(\frac{\omega}{c} \right)^2 \quad (4)$$

Additionally, the parameters used for simulations are listed in Tab 2. They imply that the software will select specific corresponding control equations, and assign initial values and control conditions to them, in order to reconstruct the conditions in the real world.

Tab 2. Simulation parameters.

Parameter	Value
Physical Model	Incompressible air, constant temperature
Incident Pressure	1 Pa
Test Range	1000 – 5000 Hz
Step	6.25 Hz
Mesh Refinement	Finer
Test Volume	560 mm × 67 mm × 77 mm (L × W × H)

Excluding the acoustic pressure boundary, the boundaries were defined to wall conditions, i.e., the normal acoustic pressure is zero. Then, user defined functions (UDF) were defined for post-processing purposes, especially to generate the insertion loss. Afterwards, a series of batch simulations were solved in COMSOL, producing the raw data of computational fields. Insertion loss is calculated by the following **Eq 5.** for comparison among different designs.

$$IL = 20 * \log \frac{P_{inc}}{P_{tran}} \quad (5)$$

It is an important parameter in acoustic research because it helps us quantify the attenuation or reduction in sound intensity that occurs when sound waves pass through or interact with a component or system (hereby is the sonic crystals array area). In both our simulation study and experiments, insertion loss serves as a critical parameter for assessing the performance of acoustic crystals.

3 Preliminary Results

Preliminary simulation results suggest that whether utilizing fractal patterns or structures with fluidic attributes, their structural advantages, when combined with sonic crystals, consistently exhibit remarkable sound shielding efficacy at specific frequencies. Nevertheless, at other frequencies, their performance primarily hinges on the arrangement of sonic crystals.

According to simulation results, the selected square split tubes design with 1.5 mm wall thickness, 3.0 mm gap distance, and 5.0 mm slot width targets a band gap

of around 2720 Hz, while the Hilbert curve sonic crystals aim at around 1440 Hz. The Tesla valve sonic crystals can generate the highest insertion loss at 2550 Hz. And the Gosper curve sonic crystals insertion loss graph has 3 peaks in the range between 1000 Hz to 3000 Hz, which are 1510 Hz, 2190 Hz, and 2310 Hz shown in **Fig 6**. Insertion loss comparisons for square split tubes with different parameters have been done shown in **Fig 7**.

Although the reasons for the differences in insertion loss and spectral response produced by them are unknown, these differences are still of interest.

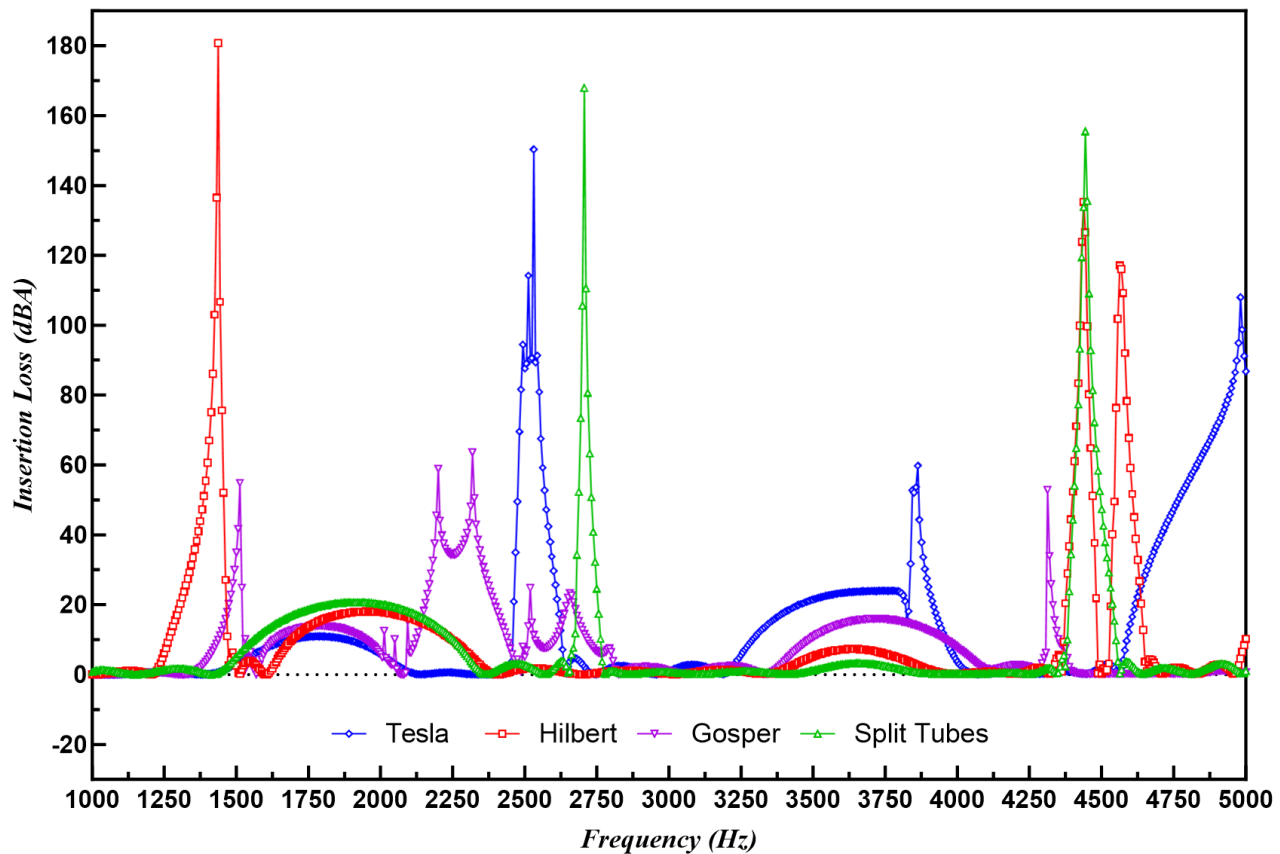


Fig 6. Insertion loss comparison between 4 types of sonic crystals.

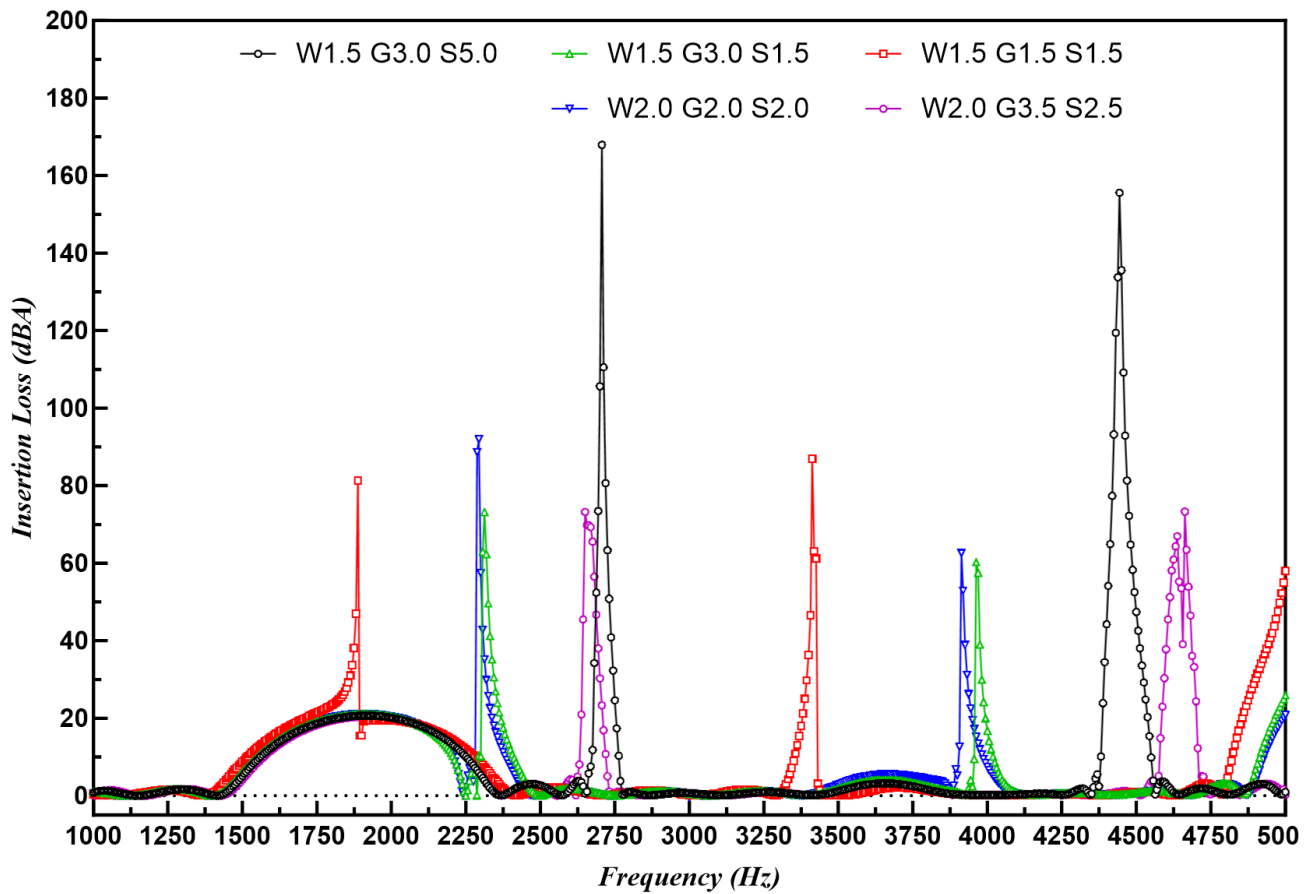


Fig 7. Insertion loss comparison for square split tubes with different geometric parameters (W: wall thickness, G: gap distance, S: slot width).

We can adjust those three parameters wall thickness, gap distance, and slot width to aim for attenuating different frequencies. Moreover, it is evident from the sound pressure contour maps that the size of gaps plays a significant role in sound dynamics. They show that changes in gap size have a notable impact on sound wave propagation, making gap size a key factor in regulating sound pressure distribution and intensity. This phenomenon arises from the differing phases resulting from the interaction of incident and reflected sound waves within varying gap dimensions. It is essential to emphasize that sound waves are essentially pressure

waves engendered by air molecules' periodic compression and rarefaction. Consequently, in narrower gaps, air molecules undergo compression, thereby exerting a discernible influence on sound pressure. Furthermore, our investigation extended to encompass the unidirectional acoustic characteristics of Tesla valves, revealing that the unidirectional attributes do not manifest prominently within the acoustic domain. Instead, both directions consistently exhibit uniform transmission losses on a certain frequency. Based on the simulations, one relatively high-performance sonic crystal out of each type was chosen for manufacturing.



Fig 8. 3D printed samples.

4 Experiment

As shown in **Fig 8**, four test models were printed. The material used for printing

was photosensitive resin, which is strong enough and has high printing accuracy to meet our needs. It performs much better compared to PLA or ABS materials used in small 3d printers. To form acoustic crystals, six of each structure were printed before the tests.

The four types of 3D-printed sonic crystals have been tested in the same layout as in the preliminary simulation shown in **Fig 9**. The C-type square slit interleave structure in different directions are also tested, shown in **Fig 10**. For the Gosper curve structure, both different layouts and different numbers have been tested shown in **Fig 11** and **Fig 12**, respectively.

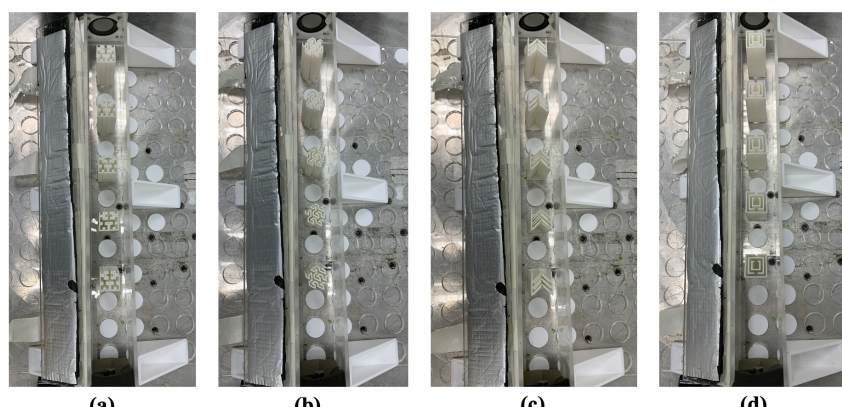


Fig 9. Real experiment layout of
(a) Hilbert curve structure, **(b)**
 Gosper curve structure, **(c)** Tesla
 valve structure, and **(d)** C-type
 square split interleave structure.
 For comparison between different
 structures.

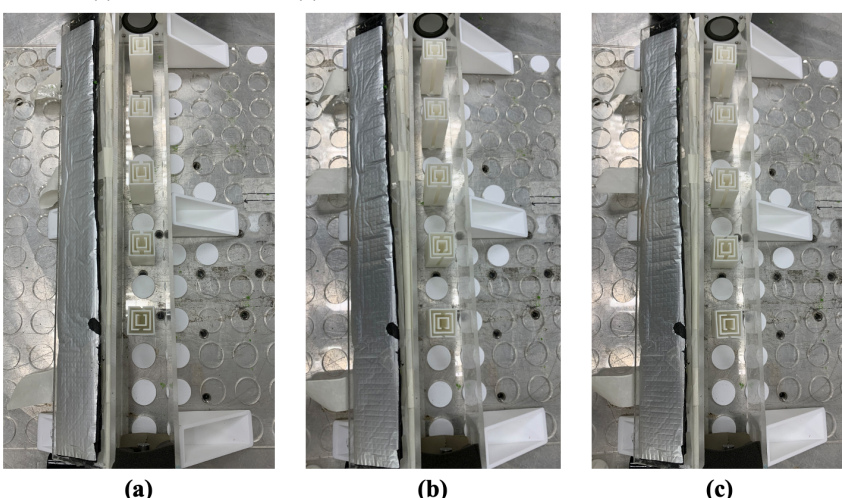
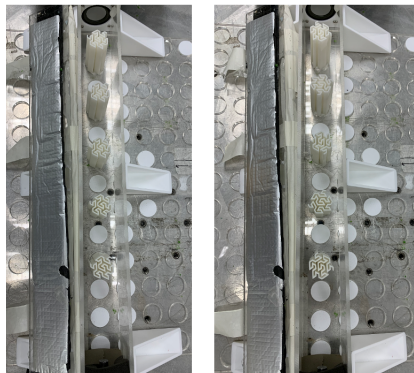
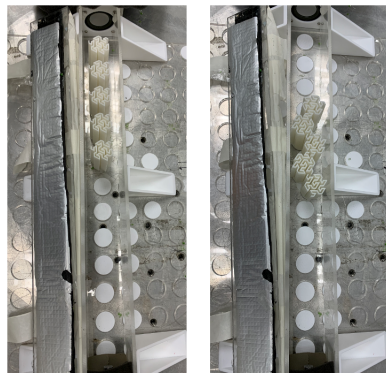


Fig 10. Different experiment
 layouts of C-type square split
 interleave structure in **(a)** same
 direction with the outer slot facing
 the speaker, **(b)** reversed direction
 with the outer slot facing the
 microphone, **(c)** different
 directions between neighboring
 two. For comparison between
 different layouts of square split
 tubes.



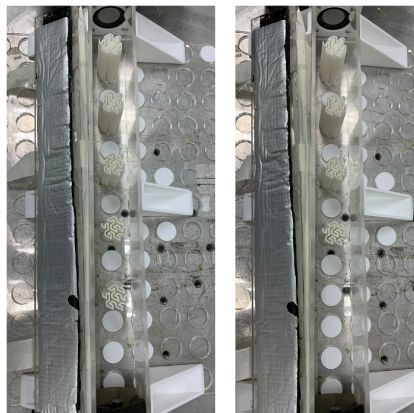
(a)



(c)

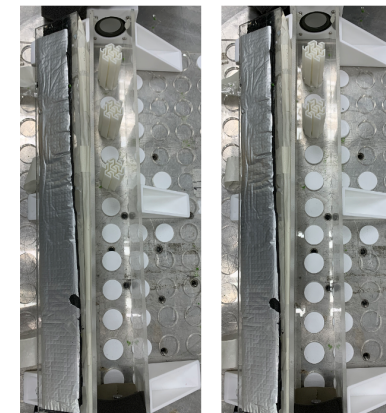
(d)

Fig 11. Different experiment layouts of Gosper curve structure in **(a)** same direction (0 deg), **(b)** different directions (each one has twisted 90 deg relative to its front counterpart), **(c)** smaller gaps, **(d)** connected shape. For comparison between different layouts of the Gosper curve structure.



(a)

(b)



(c)

(d)

Fig 12. Gosper curve structure sonic crystals with **(a)** 5 pcs, **(b)** 4 pcs, **(c)** 3 pcs, **(d)** 2 pcs. For comparison between different numbers of pieces in Gosper curve structure sonic crystals.

5 Analysis

The experiment results of insertion loss have been plotted versus frequency from 1000 Hz to 5000 Hz with a step of 6.25 Hz for all setups shown in **Fig 13** to **Fig 16**. From Fig 13, it is shown that the maximum insertion loss for all four types of structures can reach above 35 dB, which means the transmitted pressure is less than 1.78% of the incident pressure at certain frequencies. Among the four types, the Gosper curve structure sonic crystals have a maximum insertion loss of 48 dB at 2543.75 Hz. The Tesla valve structure sonic crystals reach a maximum of 42.6 dB at 2412.5 Hz. And the square slit tubes sonic crystals attain a 41.2 dB

insertion loss at 1925 Hz, while the Hilbert curve structure sonic crystals have the minimum insertion loss among the four, which is 37.57 dB at 2200 Hz. From **Fig 14a**, we can see that changing the directions of the square split tubes either in a reversed direction or letting the outer slots face each other has not changed the insertion loss too much. The overall trend of the insertion loss curve is very similar among the three layouts. They all have two band gaps for blocking the sound waves with an insertion loss of around 25 dB, one is from 1850 Hz to 2250 Hz and the other is from 4550 Hz to 4630 Hz. This means the square spit tube sonic crystals can effectively reduce the acoustic pressure of those frequencies to only 5.62% of the incident pressure.

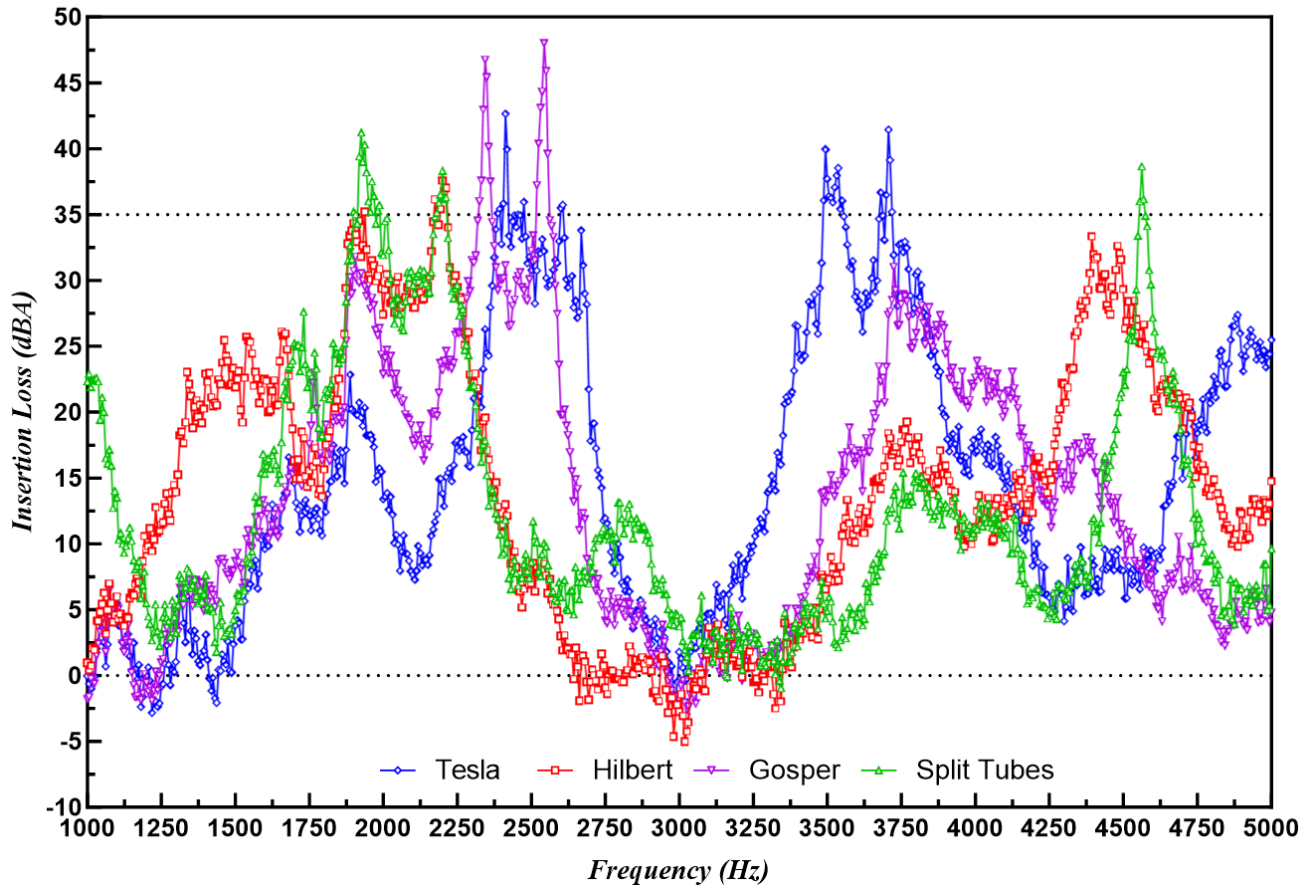


Fig 13. Experimental results of insertion loss for different shapes

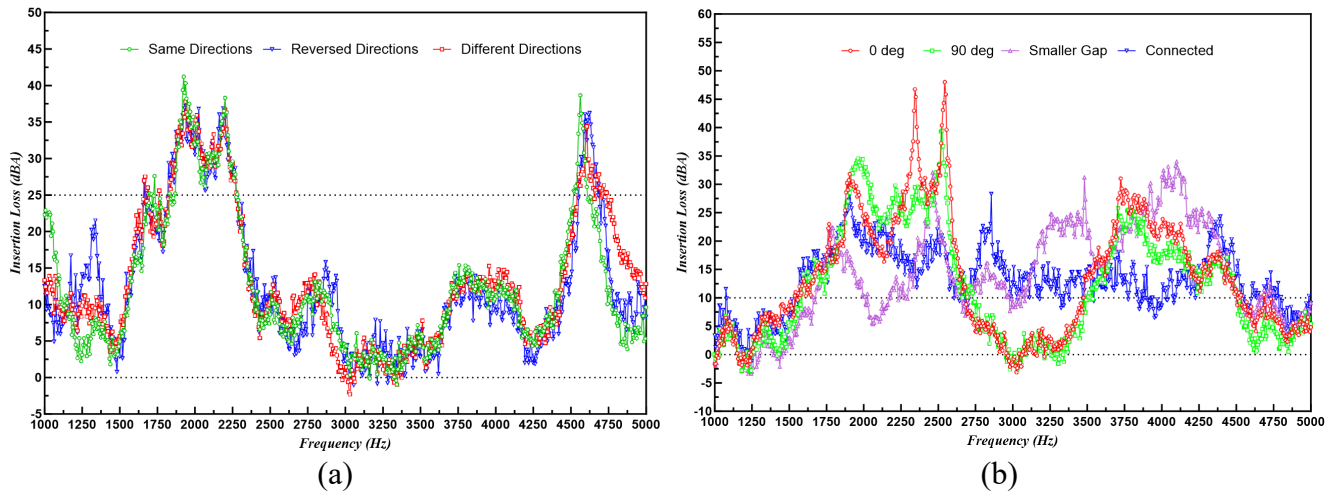


Fig 14. Experimental results of insertion loss for different layouts, (a) square split tubes, and (b) Gosper curve structures.

It can also be verified from **Fig 14b** that the center distance of the neighboring sonic crystals has a big difference in the

band gap. For the 0 deg and 90 deg, they have the same center distance, which is around 86 mm, while the smaller gap

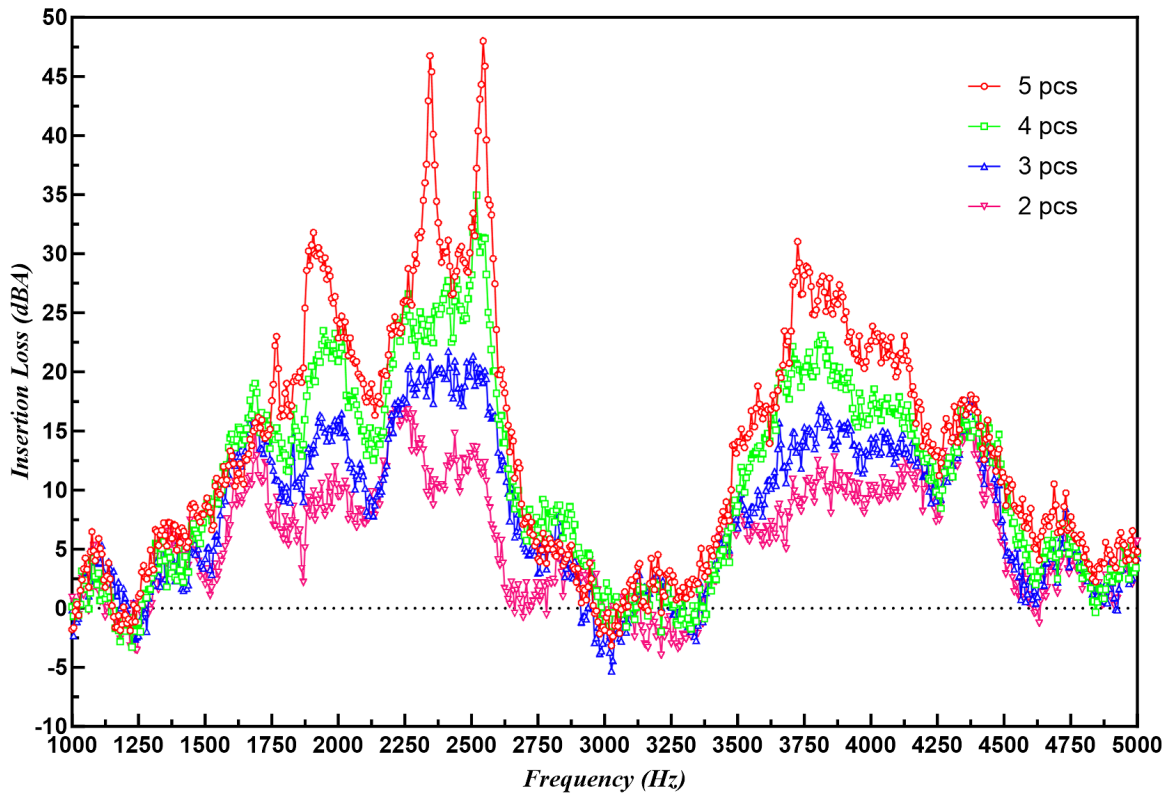


Fig 15. Insertion loss for Gosper curve structures with different numbers of pieces

sonic crystals have only half the center distance, which is around 43 mm. According to Bragg's law, the frequency that will be blocked or attenuated is around $4000n$ Hz (where $n = 1, 2, \dots$) for the smaller gap sonic crystals, while it is $2000n$ (where $n = 1, 2, \dots$) for the 0 deg and 90 deg sonic crystals. For the latter two, despite the twisted angle, the overall trend in the insertion loss curve is similar due to their same center distance. The connected Gosper curve structure, however, shows a broad band gap of more than 10 dB insertion loss almost from around 1550 Hz to 3300 Hz. It has a maximum insertion loss of 29.26 dB at 1906.25 Hz.

From **Fig 15**, we verified that with more sonic crystals in the layout, overall, the insertion loss will be higher, and the noise cancellation effect will be better at the same frequency.

Each experiment result of insertion loss is compared with its simulation counterpart. Overall, the experimental results align well with the simulation results. The total acoustic pressure is also plotted at certain frequencies for analysis.

For the Hilbert curve sonic crystals, shown in **Fig 16** the simulation aligns quite well with the simulation result. Both the simulation and experimental results have 4 main peak regions. In the simulation, the insertion loss can be up to 180 dB, while the maximum in the

experiment is only 37 dB. This is because there is a difference between the real setup and the simulation settings. The material used in the experiment is 3D printed white resin with only 1.5 mm thickness, and it is not a sound-hard material as described in the simulation. There might be other errors like the placement of the sonic crystals or measuring errors.

For the Tesla valve structure sonic crystals, the simulation also aligns quite well with the simulation result, shown in **Fig 17a**. Both the simulation and experimental results have 4 main peak regions.

At certain positions of the Helmholtz resonant cavity, the phases of the incident and reflected waves match each other, causing them to superimpose on each other to form standing waves at these positions. If the resonant cavity has one or more openings, the incident wave may be reflected through the openings. The geometry and position of the openings have an important influence on the phase of the reflected wave. In some cases, phase changes caused by opening reflections can lead to phase flips. The propagation path of sound waves in the resonant cavity may also cause phase changes. Propagation through different paths may result in a 180-degree flip in phase, especially at the resonant frequency of the cavity.

The square split tube sonic crystal (shown in **Fig 18**) has integrated the Helmholtz resonant in it, making the performance quite nice. Both the simulation and experimental results have a similar trend.

The frequency in the simulation is a bit shifted to the left compared with the experiment.

The image shows clear areas of sound pressure concentration, which represent sound waves resonating within the cavity at specific frequencies. Resonance inside the cavity usually manifests itself as sound waves repeatedly reflecting, interfering, and intensifying within the cavity at a specific frequency. The comparison of the square split tubes with reversed directions and different directions and their total sound pressure have been shown from **Fig 19-20**, which is quite similar with **Fig 18**.

The simulation results also shift to the left of the experimental result according to **Fig 21a**. Besides that, the trend is the same except for some high peaks.

The simulation results also align well with the experimental results for the 90-degree twisted case, shown in **Fig 22**.

For the Gosper curve structure sonic crystals with smaller gaps, the experimental results are shifted around 260 Hz right to the simulation results from the plot in **Fig 23**.

The connected Gosper curve structure shows a broad band gap for the experimental results (**Fig 24**). It doesn't have as high an insertion loss peak compared to other structures, but it has a very wide frequency of absorption.

Fig 25-27 show the comparison between the simulation and experimental results for Gosper curve structure sonic crystals with 4 pcs, 3 pcs, and 2 pcs, respectively. The two match quite well.

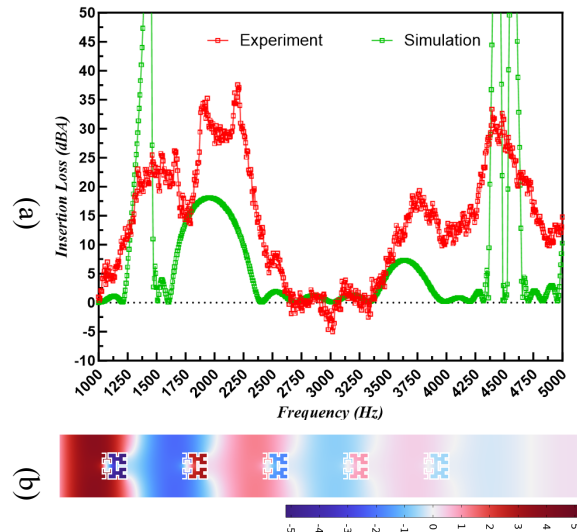


Fig 16. Hilbert curve structure sonic crystals. (a) Comparison between the experiment and simulation result of insertion loss. (b) Total acoustic pressure at 2000 Hz

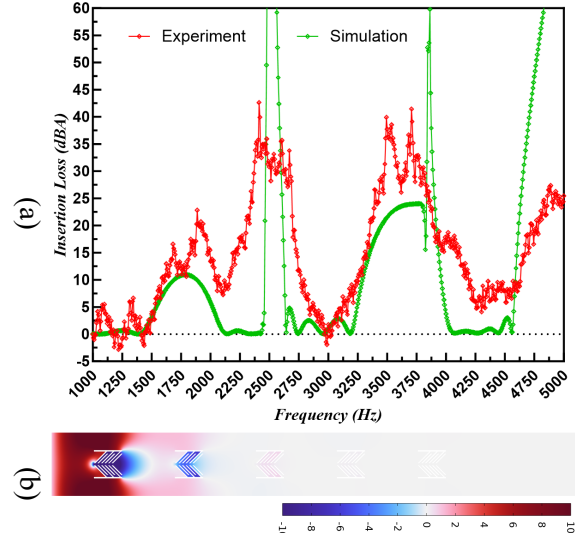


Fig 17. Tesla valve structure sonic crystals. (a) Comparison between the experiment and simulation result of insertion loss. (b) Total acoustic pressure at 2500 Hz.

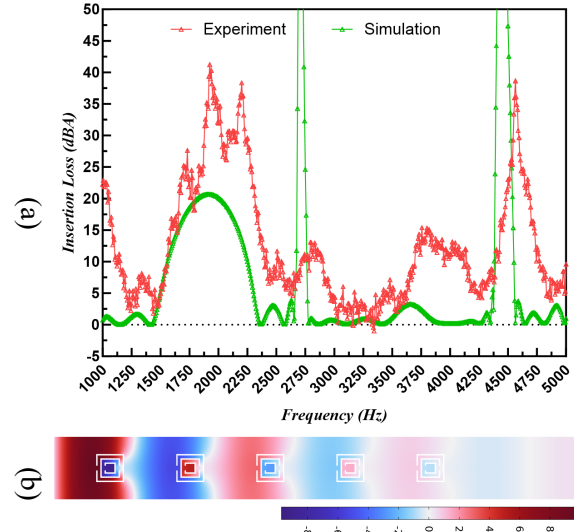


Fig 18. Square split tubes sonic crystals. (a) Comparison between the experiment and simulation result of insertion loss. (b) Total acoustic pressure at 1925 Hz

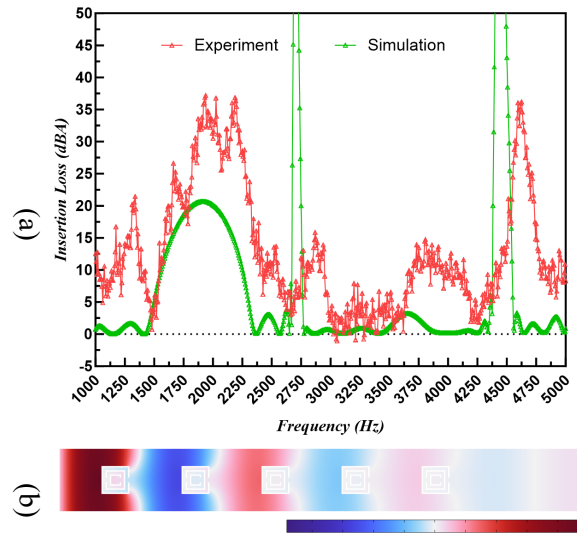


Fig 19. Square split tube sonic crystals with reversed direction. (a) Comparison between the experiment and simulation result of insertion loss. (b) Total acoustic pressure at 1925 Hz

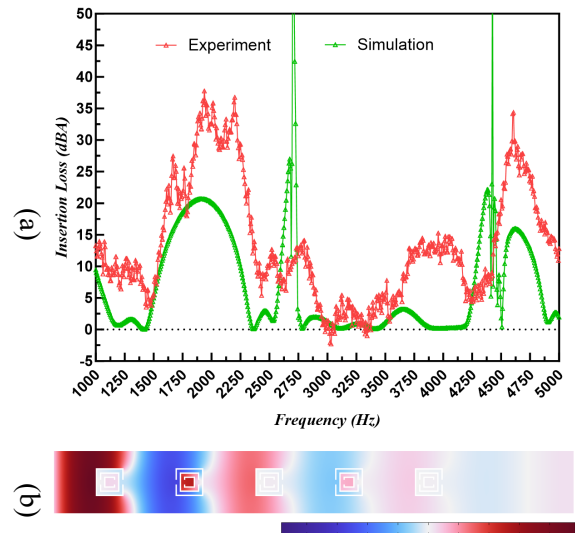


Fig 20. Square split tube sonic crystals with different directions. (a) Comparison between the experiment and simulation result of insertion loss. (b) Total acoustic pressure at 1925 Hz

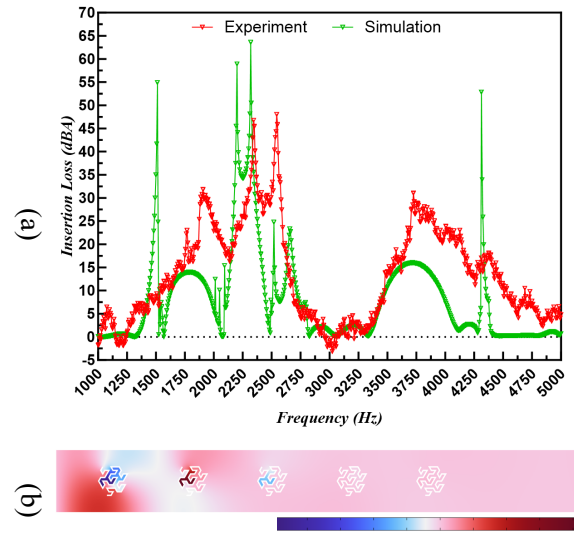


Fig 21. Gosper curve structure sonic crystals. (a) Comparison between the experiment and simulation result of insertion loss. (b) Total acoustic pressure at 2250 Hz

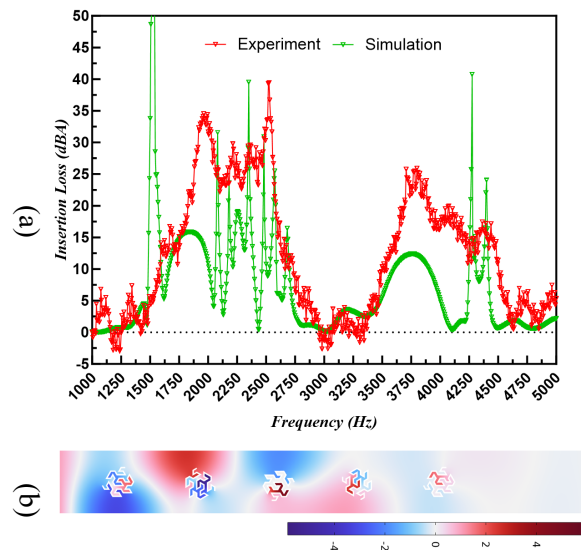


Fig 22. Gosper curve structure sonic crystals (twisted 90 deg). (a) Comparison between the experiment and simulation result of insertion loss. (b) Total acoustic pressure at 2250 Hz

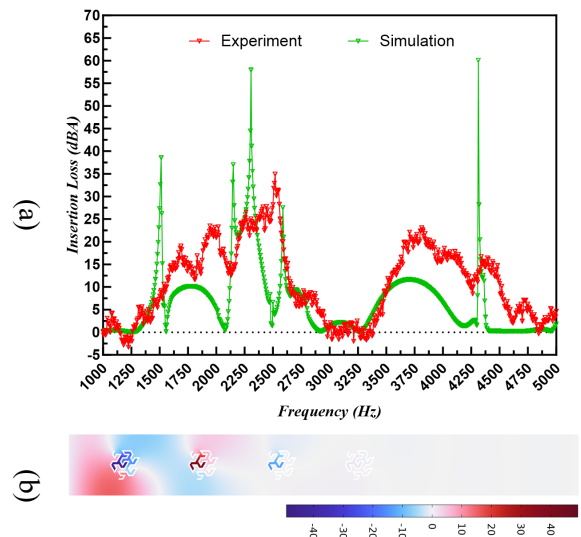


Fig 25. Gosper curve sonic crystals of 4 pcs. (a) Comparison between the experiment and simulation result of insertion loss. (b) Total acoustic pressure at 2250 Hz

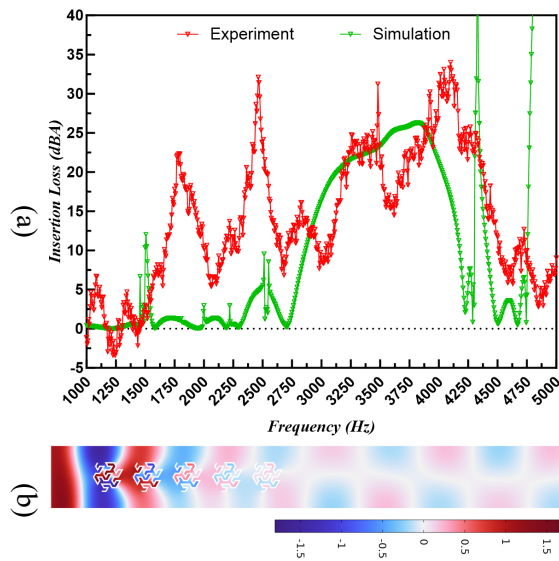


Fig 23. Gosper curve structure sonic crystals with smaller gaps. (a) Comparison between the experiment and simulation result of insertion loss. (b) Total acoustic pressure at 2250 Hz

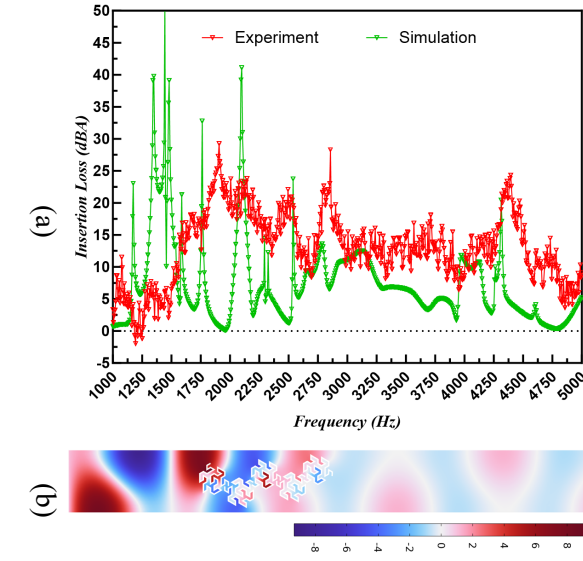


Fig 24. Connected Gosper curve structure. (a) Comparison between the experiment and simulation result of insertion loss (b) Total acoustic pressure at 3837.5 Hz

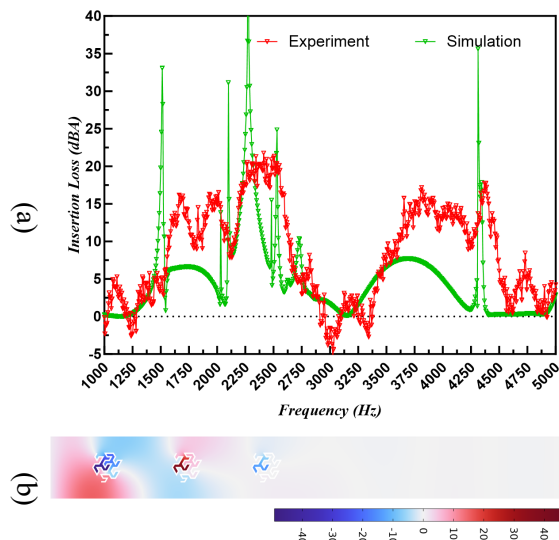


Fig 26. Gosper curve sonic crystals of 3 pcs. (a) Comparison between the experiment and simulation result of insertion loss. (b) Total acoustic pressure at 2250 Hz

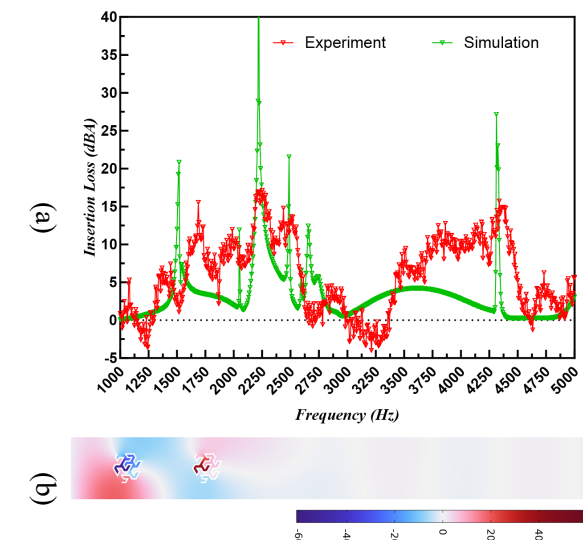


Fig 27. Gosper curve sonic crystals of 2 pcs. (a) Comparison between the experiment and simulation result of insertion loss. (b) Total acoustic pressure at 2250 Hz

Conclusion

This comprehensive study successfully demonstrated the efficacy of sonic crystals in acoustic shielding, underlying the significant role of specific structures, such as fractal patterns, fluidic attributes, and square C-type interleave shapes, in influencing sound wave dynamics. The research revealed that these structures, when combined with sonic crystals, exhibited remarkable sound shielding properties at certain frequencies. Particularly, the gaps within these structures ensemble the Helmholtz resonator and play a critical role in shaping sound pressure dynamics, owing to the interplay between incident and reflected sound waves.

The exploration of unidirectional acoustic characteristics in the square split tubes was a novel aspect of the research. These structures exhibited similar insertion loss in both directions at certain frequencies, contributing to the understanding of sonic crystal behavior in future applications.

The simulation phase using COMSOL was crucial in selecting high-performance sonic crystals for fabrication. The 3D-printed models were then subjected to rigorous testing in the Acoustic Lab, where experimental data were comprehensively collected for different setups. The close comparison with the simulation data not only validated the simulation models but also provided insights into the real-world performance of these complex structures.

From the experimental results, it was evident that each sonic crystal type had distinct sound-blocking capabilities. The Gosper curve structure, in particular, showed the highest maximum insertion loss in the experiment, highlighting its potential in targeted frequency ranges. The Tesla valve, Hilbert, and square split tube structures also demonstrated significant sound-blocking abilities, with the experimental findings aligning closely with the simulations. The study's findings are pivotal in advancing the field of acoustic metamaterials and sonic crystals and hold great potential for practical applications in noise mitigation.

References

1. Suárez, L. and M. del Mar Espinosa, Assessment on the use of additive manufacturing technologies for acoustic applications. *The International Journal of Advanced Manufacturing Technology*, 2020. 109: p. 2691-2705.
2. Gao, N., et al., Acoustic metamaterials for noise reduction: a review. *Advanced Materials Technologies*, 2022. 7(6): p. 2100698.
3. Qi, Y., et al., Acoustic realization of quadrupole topological insulators. *Physical Review Letters*, 2020. 124(20): p. 206601.

4. Qin, X., et al., Numerical modeling and field test of sonic crystal acoustic barriers. *Environmental Science and Pollution Research*, 2023. 30(6): p. 16289-16304.
5. Laxmi, V., C. Thakre, and R. Vijay, Evaluation of noise barriers based on geometries and materials: a review. *Environmental Science and Pollution Research*, 2022: p. 1-17.
6. Sun, M., et al., Broadband acoustic ventilation barriers. *Physical Review Applied*, 2020. 13(4): p. 044028.
7. Li, N., F. Wang, and G. Song, New entropy-based vibro-acoustic modulation method for metal fatigue crack detection: An exploratory study. *Measurement*, 2020. 150: p. 107075.
8. Bai, Y., et al., Acoustic-based sensing and applications: A survey. *Computer Networks*, 2020. 181: p. 107447.
9. Birnie, L., et al. Sound source localization in a reverberant room using harmonic based MUSIC. in ICASSP 2019-2019 IEEE International Conference on Acoustics, Speech and Signal Processing (ICASSP). 2019. IEEE.
10. Shtrepi, L. and A. Prato, Towards a sustainable approach for sound absorption assessment of building materials: Validation of small-scale reverberation room measurements. *Applied Acoustics*, 2020. 165: p. 107304.
11. Li, J., X. Wen, and P. Sheng, Acoustic metamaterials. *Journal of Applied Physics*, 2021. 129(17).
12. Liu, J., H. Guo, and T. Wang, A review of acoustic metamaterials and phononic crystals. *Crystals*, 2020. 10(4): p. 305.
13. Fredianelli, L., L.G. Del Pizzo, and G. Licita, Recent developments in sonic crystals as barriers for road traffic noise mitigation. *Environments*, 2019. 6(2): p. 14.
14. Vasileiadis, T., et al., Progress and perspectives on phononic crystals. *Journal of Applied Physics*, 2021. 129(16).
15. Miyashita, T., Sonic crystals and sonic wave-guides. *Measurement Science and Technology*, 2005. 16(5): p. R47.
16. Alagoz, S., O.A. Kaya, and B.B. Alagoz, Frequency-controlled wave focusing by a sonic crystal lens. *Applied Acoustics*, 2009. 70(11-12): p. 1400-1405.
17. Lu, J., et al., Observation of topological valley transport of sound in sonic crystals. *Nature Physics*, 2017. 13(4): p. 369-374.
18. Martínez-Sala, R., et al., Control of noise by trees arranged like sonic crystals. *Journal of sound and vibration*, 2006. 291(1-2): p. 100-106.
19. Kragh, J., Road traffic noise attenuation by belts of trees. *Journal of Sound and Vibration*, 1981. 74(2): p. 235-241.
20. Hu, X., C.T. Chan, and J. Zi, Two-dimensional sonic crystals with Helmholtz resonators. *Physical Review E*, 2005. 71(5): p. 055601.
21. Dimitrijević, S.M., et al., Sound insulation and reflection properties of sonic crystal barrier based on micro-perforated cylinders. *Materials*, 2019. 12(17): p. 2806.

-
- 22.Ho, K.M., et al., Broadband locally resonant sonic shields. *Applied physics letters*, 2003. 83(26): p. 5566-5568.
 - 23.Cai, X., et al., Ultrathin low-frequency sound absorbing panels based on coplanar spiral tubes or coplanar Helmholtz resonators. *Applied Physics Letters*, 2014. 105(12).
 - 24.Xie, Y., et al., Tapered labyrinthine acoustic metamaterials for broadband impedance matching. *Applied Physics Letters*, 2013. 103(20).
 - 25.Akiwate, D.C., et al., Acoustic properties of additive manufactured narrow tube periodic structures. *Applied Acoustics*, 2018. 136: p. 123-131.
 - 26.Comandini, G., et al. Hilbert Fractal Metamaterials for lightweight sound insulation. in e-Forum Acusticum 2020. 2020.
 - 27.Man, X., et al., Hilbert fractal acoustic metamaterials with negative mass density and bulk modulus on subwavelength scale. *Materials & design*, 2019. 180: p. 107911.
 - 28.Guild, M.D., et al., 3D printed acoustic metamaterial sound absorbers using functionally-graded sonic crystals. European Acoustics Association, 2018.
 - 29.Wu, P., et al., Acoustic absorbers at low frequency based on split-tube metamaterials. *Physics Letters A*, 2019. 383(20): p. 2361-2366.
 - 30.Anguera, et al., Fractal Antennas: An Historical Perspective. *Fractal and Fractional*, 2020. 4(1).